





Sorting of extremely small nanoparticles by membranes supporting symmetry-protected bound states in the continuum

Evgeny Bulgakov ¹, Galina Shadrina,² Almas Sadreev ¹ and Konstantin Pichugin ^{1,*}

¹*Kirensky Institute of Physics, Federal Research Center KSC SB RAS, 660036 Krasnoyarsk, Russia*

²*Institute of Computational Modelling SB RAS, 660036 Krasnoyarsk, Russia*

 (Received 26 February 2024; revised 25 July 2024; accepted 29 July 2024; published 16 August 2024)

We consider double perforated slabs (membranes) that support a symmetry-protected bound state in the continuum (BIC). These slabs are immersed into a liquid at room temperature. Laser excitation of the BIC generates giant optical forces that strongly affect the Brownian motion of nanoparticles in a colloidal solution. By solving of the Fokker-Planck equation we show that a single membrane can localize only larger nanoparticles. However, system of two parallel membranes can trap extremely small nanometer-sized nanoparticles by a resonant excitation of quasi-BICs, with varying intensities in each membrane.

DOI: [10.1103/PhysRevB.110.075305](https://doi.org/10.1103/PhysRevB.110.075305)

I. INTRODUCTION

The precise and efficient sorting of specific target molecules from complex mixtures is fundamentally important for many applications. The standard molecular sorting relies heavily on centrifugation and filtration for their simplicity and high throughput, but has low accuracy, poor recovery, and large sample requirements [1]. Among the various sorting methods, optical sorting, which exploits the different optical and/or fluid drag forces on different objects [2], is particularly attractive because of its great potential for precise separation of nanoscale objects [3]. The optical power could be easily localized to achieve efficient light-matter interactions, so that the optical force is even sufficient to sort nanometer-sized molecules. This localization is achieved by the excitation of resonant modes with small mode volume and sufficient intensity enhancement, such as surface plasmons or high- Q resonant modes in chips and photonic crystal (PhC) structures [2,4–14], particularly whispering gallery modes (WGMs) [15–18] in cylindrical resonators or guided modes [19–21] in PhC waveguides. Furthermore, the optical force is highly sensitive to particle properties, size, and refractive index that are of key importance for sorting.

Along with the high- Q modes outlined above, bound states in the radiation continuum (BICs) offer a promising way to manipulate and sort nanoparticles [17,22–35]. In particular, different types of BICs, symmetry protected (SP), Friedrich-Wintgen, accidental, and Fabry-Perot, have been observed in membranes [36–43]. In the present paper, we employ the SP BICs because of their robustness to material and structural fluctuations [44].

The proposed structure comprises two perforated slabs (membranes), as illustrated in Fig. 1. The excitation of a quasi-BIC in the membranes by an incident laser beam gives rise to a giant Ashkin optical potential well whose depth is

proportional to the polarizability of the nanoparticle and the intensity of the beam. This potential is periodic along the membrane but localized across it. The Brownian motion of nanoparticles along the periodic potential and the respective sorting were subjects of numerous studies [2,45–48]. In the present paper, we consider sorting of nanoparticles based on their Brownian motion across two membranes, as illustrated in Fig. 1. These membranes generate two optical potential wells of different depths, as a result of the excitation of quasi-BICs in the membranes. The depths of the optical potentials are controlled by two laser beams independently.

Initially, nanoparticles of various sizes but with an identical permittivity are distributed uniformly on the left of the membranes. The optical potential induced by the resonant mode depends on the size of the particles and, thus, the diffusion times across the membrane depends on the particle size. This results in a time-dependent probability distribution over particle size in different regions of the system. The smaller particles are able to pass freely through the first (left) membrane, while the optical potential for larger particles is much deeper, resulting in their trapping and formation of a smooth step-like distribution of the nanoparticle sizes in the membrane holes. The next (right) membrane, in which the same SP quasi-BIC is excited but with a deeper optical potential, traps larger particles, which are small enough to pass through the left membrane.

In this study, perforated membranes are employed as they permit the free passage of nanoparticles up to hundreds of nanometers in size. To simplify calculations, the nanoparticles are assumed to be spherical, isotropic, and of very small size, ranging from a nanometer to a few nanometers. These sizes were selected as an example of an extreme case for optical sorting. In fact, the potential must be deep enough to trap such a small particle. Sorting different types of fullerenes could be proposed as a practical application. Of course, the method is not limited to very small nanoparticles. The size of the sorted particles is controlled by the laser powers, W_L and W_R , which can be varied over a wide range.

*Contact author: knp@tnp.krasn.ru

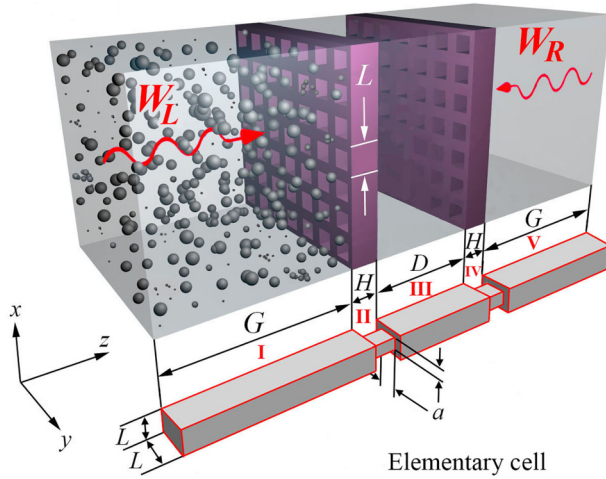


FIG. 1. Double silicon membranes with the permittivity $\varepsilon = 12$ submerged in water with the refractive index 1.33. At initial time spherical nanoparticles of different radii r_p but equaled permittivity $\varepsilon_p = 3$ are distributed homogeneously at the left side of the left membrane. Laser beams of the same frequency but different powers resonantly excite SP BICs supported by membranes as sketched by red wavy lines.

II. SYMMETRY-PROTECTED BOUND STATES IN THE CONTINUUM IN ONE MEMBRANE

For the convenience of the reader all the dimensions of the membrane are depicted in the bottom of Fig. 1. The following membrane parameters were selected: period $L = 1082$ nm, square holes of size $a \times a$, where $a = 703$ nm, and slab thickness $H = 1082$ nm. With these dimensions, the membrane supports a number of SP BICs in the Γ point. In this study, we will select the SP BIC with the maximal electromagnetic (EM) field intensity inside the membrane holes. The field distribution of this SP BIC with the eigenfrequency $\omega_c L/c = 4.3505$, calculated using COMSOL MultiPhysics, is shown in Fig. 2.

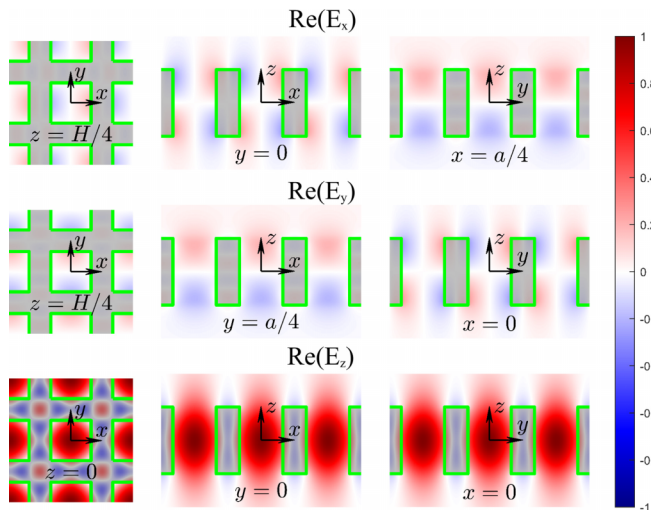


FIG. 2. EM field components of the SP BIC solution of an infinitely periodic silicon membrane immersed in water with the eigenfrequency $\omega_c L/c = 4.3505$. The dielectric of the membrane is shown in gray.

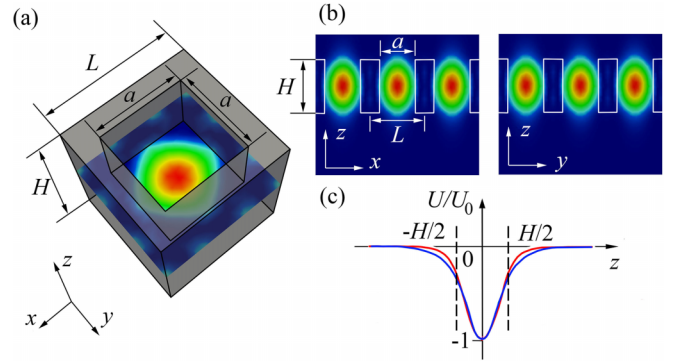


FIG. 3. The EM field intensity $|\mathbf{E}(x, y, z)|^2$ of the SP BIC solution, which determines the optical potential (1). The intensity in the cross section $x, y, z = 0$ (a). The dielectric of the membrane is displayed in grey. The intensity in the cross sections $x, z, y = 0$ and $y, z, x = 0$ (b). The optical potential along the z axis at $x = y = 0$ (c) (red line) is compared to the model potential $-U_0/\cosh(\delta z/H)$ in Eq. (5) for the $r_p = a$ and fitting parameter $\delta = 3.7$ (blue line). U_0 represents the maximum depth of the optical potential in the left membrane. The origin of the coordinate system is at the center of the left membrane hole.

The corresponding optical potential is presented in Fig. 3. The sizes of the system were chosen so that the SP BIC could be excited by a laser with a wavelength of $\lambda = 1.55$ μm . At this wavelength, the material losses in both silicon, from which the membrane is made, and water are negligible. In what follows we will assume that laser beams have the specified wavelength.

Excitation of the SP BIC by a resonant external laser beam illuminating membranes at normal incidence results in a giant intensity $|\mathbf{E}(x, y, z)|^2$ of the EM field. The EM field intensity enhancement is quantified by the ratio of the intensities of the incident and excited fields. This enhancement is of the same order of magnitude as the quality factor. Although the quality factor $Q = \text{Re}(\omega_c)/2\text{Im}(\omega_c)$ of SP BIC is theoretically infinite, in practice it is always finite owing to a number of causes, such as deviation from the normal incidence, the finite membrane size, structural fluctuations, material losses, and so forth, which transform BIC into quasi-BIC. In what follows we take $Q = 10^5$ to be definite.

The optical potential, which is proportional to the intensity of the EM field, can be expressed in the following form [49]:

$$U(x, y, z) = -\pi r_p^3 \frac{\varepsilon_p - \varepsilon_l}{\varepsilon_p + 2\varepsilon_l} |\mathbf{E}(x, y, z)|^2. \quad (1)$$

Here, r_p is the radius of the spherical particle with a permittivity ε_p , while ε_l denotes the permittivity of the liquid. Since the contribution of the quasi-BIC field is dominant compared to the incident wave [26], we can approximate the EM field in the Eq. (1) by the SP BIC field normalized according to the intensity enhancement.

III. BROWNIAN MOTION OF NANOPARTICLES IN THE PRESENCE OF OPTICAL FORCE

The time evolution of the probability density $P(\mathbf{r}, t)$ of spherical nanoparticles with radius r_p and permittivity $\varepsilon_p = 3$ in a liquid medium in the presence of the

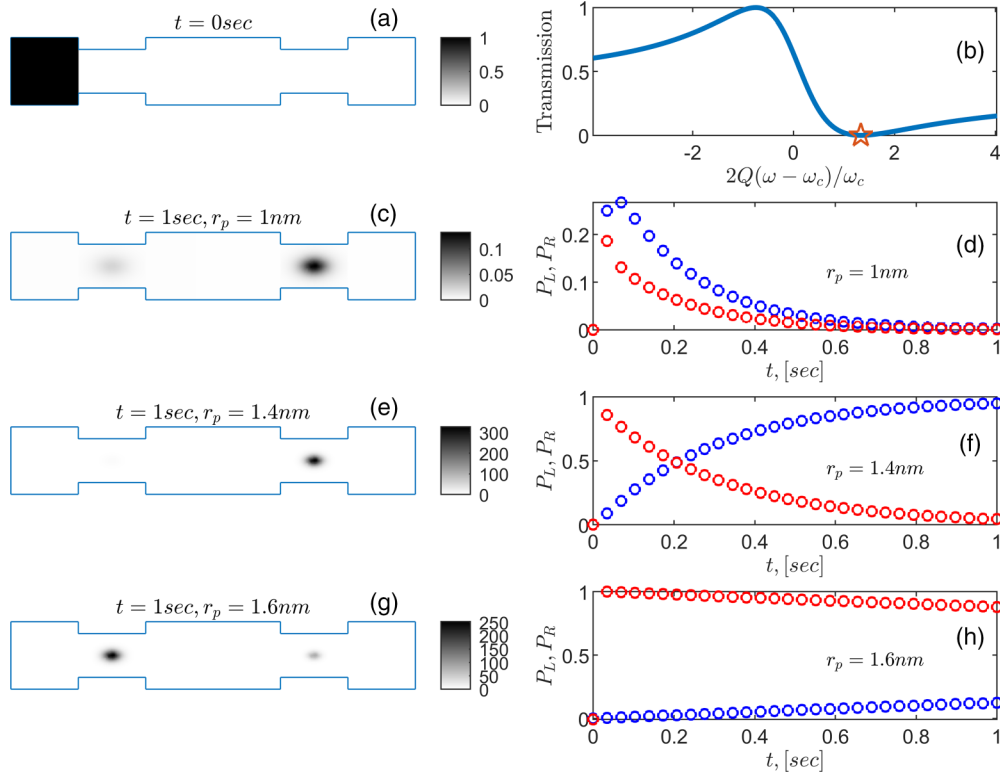


FIG. 4. Probability density of $P(x = 0, y, z)$ at initial time (a), and one second after the start of sorting for three sizes: $r_p = 1$ nm (c), $r_p = 1.4$ nm (e), $r_p = 1.6$ nm (g), where the blue line outlines the space accessible to particles. The corresponding probabilities (3) P_L (red open circles) and P_R (blue open circles) to be trapped by membranes are shown in subplots (d), (f), and (h) as a function of time. Subplot (b) shows asymmetric Fano resonance in transmission through a single membrane vs frequency $2Q(\omega - \omega_c)/\omega_c$, where $\omega_c = 4.3505c/L$ is the eigenfrequency of the SP quasi-BIC with $Q = 10^5$. Zero transmission point is marked by star.

Ashkin force $\mathbf{F} = -\nabla U(\mathbf{r})$ satisfies the Fokker-Planck equation [50–52]

$$\begin{aligned} \frac{dP}{dt} &= \frac{1}{\gamma} (-\nabla(P\mathbf{F}) + k_B T \nabla^2 P) \\ &= \frac{H^2}{t_0} \left(\nabla \left(P \nabla \frac{U(\mathbf{r})}{k_B T} \right) + \nabla^2 P \right), \end{aligned} \quad (2)$$

where $U(\mathbf{r})$ is the optical potential (1), $\gamma = 6\pi\eta r_p$ is the friction coefficient, $t_0 = \frac{\gamma H^2}{k_B T}$ is the characteristic diffusion time in the system, $T = 300$ K is the temperature of water with permittivity $\epsilon_l = 1.33^2$, and $\eta = 0.0009$ Pa sec is the dynamic viscosity of water. The characteristic time t_0 is proportional to the particle size r_p , which means that small particles in a liquid reach thermodynamic equilibrium faster than the larger ones.

Our system consists of two identical membranes. Both membranes are illuminated by laser beams polarized along the x axis from the opposite sides. However, the left and right beams have different powers W_L and W_R , respectively, as sketched in Fig. 1. We assume that the beams are tuned to the frequency at which the light transmission through each membrane is zero [40,43,53], as a result of the asymmetric Fano resonance [54–56]. The Fano resonance corresponds to interference of two resonances, one broad and one narrow. For such an interaction, the points corresponding to maximum and zero transmission appear on the transmission coefficient plot, as in Fig. 4(b). These points are separated by a gap comparable with the width of the narrow resonance, so by

tuning the transmission to zero we still excite the quasi-BIC. The total-reflection requirement ensures that the laser beam on the left excites the quasi-BIC only in the left membrane and does not affect the right membrane and *vice versa*. The cross-talk effect, which significantly reduces the controllability of the sorting process, can also be avoided by using slightly different membranes and exciting quasi-BIC in each membrane at different wavelengths.

Since the optical potential and the initial conditions for the probability density are periodic, it is sufficient to solve Eq. (2) in the unit cell shown in the bottom of Fig. 1 with appropriate boundary conditions. The absence of a probability flow across the unit cell boundaries corresponds to the Neumann boundary condition $dP/dn = 0$, which is used in the calculations.

In Fig. 1 five regions of the system are marked. Regions II and IV contain membranes that generate the optical potential. In the other regions I, III, and V, the potential is negligibly small. For solving Eq. (2), the distances shown in Fig. 1 were chosen as $G = H$, $D = 2H$.

We assume, that at the initial time $t = 0$ all nanoparticles of different sizes fill the region I only. Figure 4(a) shows the density probability cross section $P(x = 0, y, z, t = 0)$ that satisfies the normalization condition $\int P(\mathbf{r}, t = 0) dV = 1$. The initial condition is far from equilibrium, so the particles undergo Brownian motion towards the other regions. If there were no optical forces, the particles after reaching thermodynamic equilibrium would be homogeneously distributed in all regions. Upon the resonant excitation of the quasi-BIC, the

Brownian motion of the particles is undergoing a significant change if the depth of the optical potential (1) is comparable to the thermal energy $k_B T$. For a quasi-BIC quality factor of $Q = 10^5$ and incident power of order of $10 \text{ mW}/\mu\text{m}^2$, the Ashkin force competes with the Brownian force at $r_p \sim 1 \text{ nm}$. This causes larger particles to be trapped by the Ashkin potential and the smaller particles to pass through the membrane. The optical potential (1) tends to localise particles inside the membrane holes, where it reaches a minimal value. Since the potential (1) is proportional to r_p^3 , the Brownian motion process is strongly dependent on the size of the particles. The solution of Eq. (2) is illustrated in subplots of Fig. 4 for the incident plane wave intensities of $W_L = 14 \text{ mW}/\mu\text{m}^2$ and $W_R = 23.3 \text{ mW}/\mu\text{m}^2$ for the particle sizes of $r_p = 1 \text{ nm}$, 1.4 nm , and 1.6 nm at the time of one second after the start of the sorting process.

Note that very small particles are not affected by the optical potential and easily penetrate into region V during the one second time interval, and it is reasonable to remove them from region V, for example by a slow flow of liquid parallel to the membranes. In the modeling, this is achieved by introducing into the right-hand side of Eq. (2) a relaxation term $-\mu P$, which acts only in region V.

To estimate the probability of particle trapping by membranes, we introduce the following quantities:

$$\begin{aligned} P_L(t) &= \int_{II} P(\mathbf{r}, t) dV, \\ P_R(t) &= \int_{IV} P(\mathbf{r}, t) dV, \end{aligned} \quad (3)$$

where integration is performed only over region II or IV. As illustrated in Figs. 4(d), 4(f), and 4(h), the probabilities $P_L(t)$ and $P_R(t)$ exhibit distinct behaviors crucially dependent on the radius of the particles. For a particle sizes less than $r_p = 1 \text{ nm}$, the probability $P_{L,R}$ in regions II and IV is notably low because of the inability of the optical potential to trap the particles. Consequently, they have migrated to region V and have left the structure because of the relaxation term. In contrast, for $r_p = 1.4 \text{ nm}$ the particles are mostly trapped in region IV. For a particle size of $r_p = 1.6 \text{ nm}$, the majority of particles was unable to reach region IV within one second and were instead localized on the left membrane. This observation demonstrates a clear effect of particle sorting by size.

In order to gain a deeper insight into the underlying physics of the observed phenomenon we consider a one-dimensional version of Eq. (2),

$$\frac{dP}{dt} = \frac{H^2}{t_0} \left(\frac{d}{dz} \left(P \frac{dU(z)}{dz k_B T} \right) + \frac{d^2}{dz^2} P \right). \quad (4)$$

The presence of membranes is modelled by a one-dimensional potential with two wells positioned at $z_L = 0$ and $z_R = D + H$. This potential is approximated by the empirical formula

$$U(z) = -U_{0L} \frac{(r_p/\alpha)^3}{\cosh(\delta(z - z_L)/H)} - U_{0R} \frac{(r_p/\alpha)^3}{\cosh(\delta(z - z_R)/H)}, \quad (5)$$

where δ is the fitting parameter and $U_{0L,0R}$ is the depth of the optical potential in the left and right membranes for $r_p = \alpha$.

Here we introduce the value α , which corresponds to the characteristic size of the sorted particles. The parameter α is used to relate the potential depth, which is assumed to be of order of several $k_B T$, to a specific value of r_p . A sketch of the potential (5) is shown in the inset of Fig. 5(d). Equation (4) was solved with the Neumann boundary conditions. The initial condition is defined by the following relations $P(z < z_L - H/2, t = 0, r_p) = \text{const}$, $P(z > z_L - H/2, t = 0, r_p) = 0$, $\int P dz = 1$.

Note that the real optical potential has a minimum in the center of the membrane hole and is increasing towards its edges. The corresponding force always has a component directed towards the z axis. The probability density also exhibits maximal values in the vicinity of the z axis, which justifies the use of the one-dimensional approximation. The approximating function $1/\cosh$ in the potential (5) was chosen because of its exponentially decaying tails, as observed in the real potential. A comparison of the real potential and the one-dimensional approximation with the parameter $\delta = 3.7$ shows perfect agreement as seen in Fig. 3(c).

First, let us see how each potential well individually affects the Brownian motion of particles of size r_p . For this purpose we need to solve Eq. (4) for the potential (5) with $U_{0L} \neq 0, U_{0R} = 0$ and with $U_{0L} = 0, U_{0R} \neq 0$. We denote the corresponding localization probabilities (3) by $P_L^1(t, r_p)$ and $P_R^1(t, r_p)$. The results of the calculations are presented in Figs. 5(a) and 5(b), which show that larger particles are almost completely trapped, while smaller particles pass freely through the membrane. The crossover between these two regimes occurs near the line $P_{L,R}^1(t, r_p) = 0.5$. Obviously, the crossover line strongly depends on the depth of the potential $U_{0L}/k_B T, U_{0R}/k_B T$ and shifts towards the region of smaller sizes r_p when the potential is increased.

Next, consider the joint effect of both potentials under condition $U_{0R} > U_{0L}$. Then, the particles able to pass the left potential well will be captured by the stronger right potential well, while the smallest particles are affected by neither well and will leave the sorting region as a result of the relaxation term. A simple estimate indicates that particles are outside the left membrane with probability $(1 - P_L^1(t, r_p))$ and will be captured by the right membrane with probability $P_R^1(t, r_p)$. Then, the probability to be trapped in the right membrane for the case of double potential well can be approximated as $P_R(t, r_p) \approx (1 - P_L^1(t, r_p))P_R^1(t, r_p)$.

Figures 5(c) and 5(d) show the dependence of the localization probability in the right membrane on time and size of the particles. Figure 5(c) shows the case of a simple multiplication of the probabilities while Fig. 5(d) shows the result of solving the one-dimensional Fokker-Planck equation (4) with the double-well potential. The probability $P_R(t, r_p)$ exhibits a pronounced maximum. The maximal probability value tends to 1 as time increases for fixed $r_p(t)$. In other words, particles with size close to $r_{p0}(t)$ are trapped by the right potential well with some distribution. This is the key idea of sorting. The result obtained by simple multiplication of probabilities well agrees with the exact solution as can be seen in Figs. 5(c) and 5(d). A more detailed picture of the time evolution of $P(z, t)$ is given in Fig. 6 for four particle sizes $r_p = 1\alpha, 1.3\alpha, 1.45\alpha$, and 1.6α .

Our studies show, see Fig. 7, that both the width of the distribution function and the maximum value depend strongly on

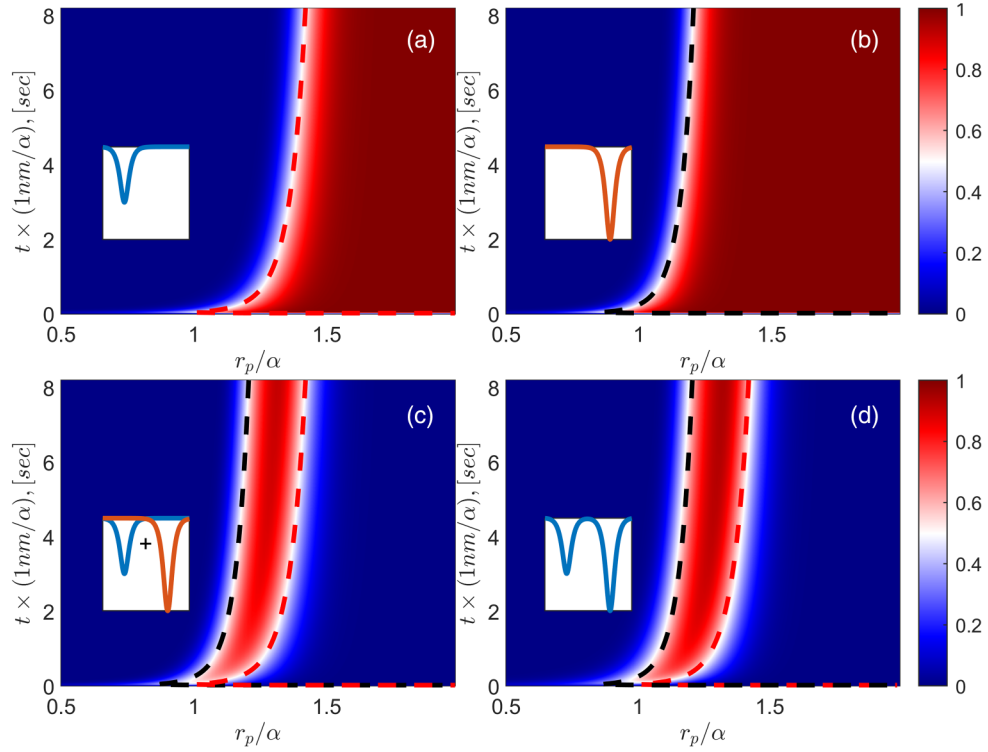


FIG. 5. Solutions of the one-dimensional Fokker-Planck equation (4) with potential (5). Localization probability $P_L^1(t, r_p)$ in one potential well with $U_{0L} = 3k_B T, U_{0R} = 0$ (a). Localization probability $P_R^1(t, r_p)$ in one potential well with $U_{0L} = 0, U_{0R} = 5k_B T$ (b). The case of two potential wells: the probability of localization in the right membrane by approximate theory $P_R(t, r_p) = (1 - P_L^1(t, r_p))P_R^1(t, r_p)$ (c), the probability of localization in the right membrane $P_R(t, r_p)$ in the case of two potential wells (d). The red dashed line corresponds to the equation $P_L^1(t, r_p) = 0.5$, the black dashed line corresponds to the same, but for the probability $P_R^1(t, r_p)$. The vertical axis represents the value $t \times (1 \text{ nm}/\alpha)$, where α is the characteristic size defined below Eq. (5).

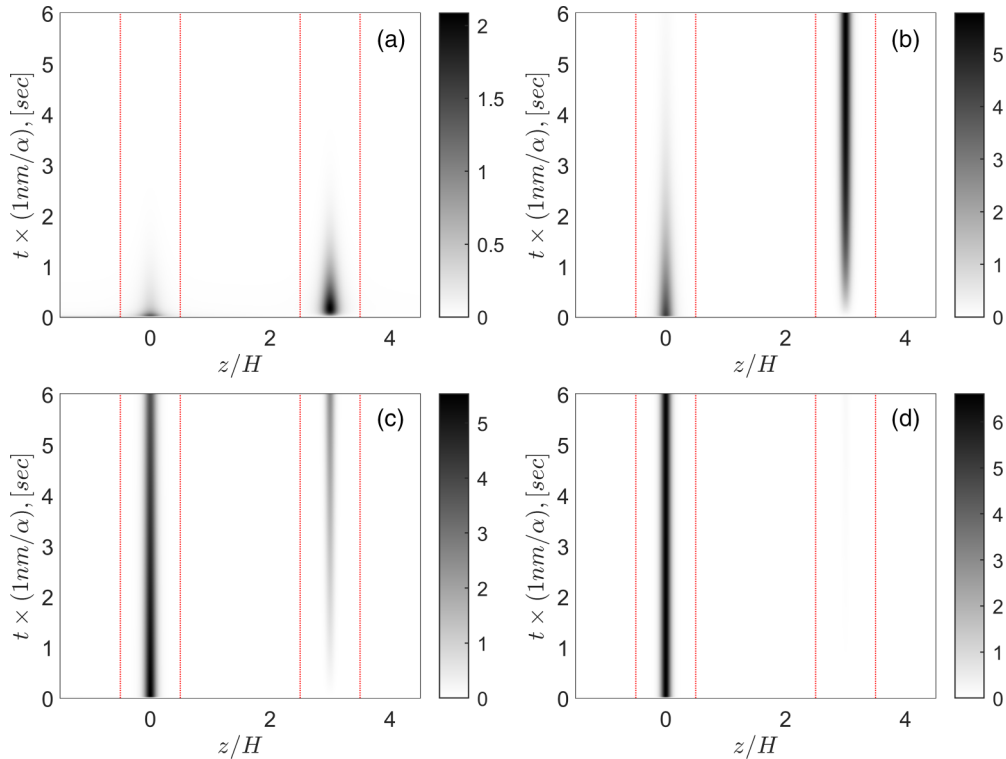


FIG. 6. Behavior of the solution of the one-dimensional Fokker-Planck equation (4) $P(z, t)$ for different particle sizes: $r_p = 1\alpha$ (a), $r_p = 1.3\alpha$ (b), $r_p = 1.45\alpha$ (c), and $r_p = 1.6\alpha$ (d). The membrane boundaries are indicated by red dotted lines.

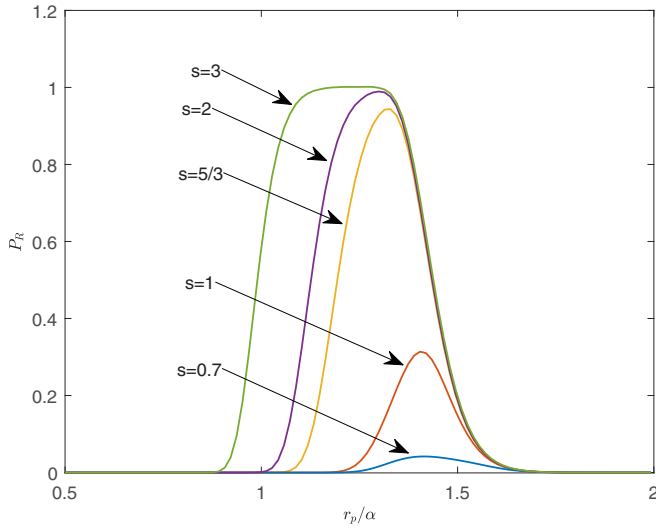


FIG. 7. Probability distribution P_R (3) of the one-dimensional model (4) with a double-well potential (5) over the sizes r_p/α at the time $t = 1 \text{ sec} \times (\alpha/1 \text{ nm})$ depending on the ratio $s = U_{0R}/U_{0L}$.

the ratio U_{0R}/U_{0L} . If we assume that the distribution should be narrow enough with a sufficiently high peak, then $U_{0R}/U_{0L} = 5/3$ can be chosen as the optimal ratio. The maximum of the probability distribution $P_R(t, r_p)$ resulting from the inequilibrium of the process undergoes a continuous shift in the

course of time. Therefore, the sorting is complete in a fixed moment of time, say $t = 1 \text{ sec} \times (\alpha/1 \text{ nm})$. After that, the mechanism of removing the sorted particles from the right membrane is to be switched on. In our example shown in Fig. 5(d), the probability of localization in the right membrane $1 \text{ sec} \times \alpha/1 \text{ nm}$ after the start of sorting P_R reaches a maximum for the size $r_p \approx 1.4\alpha$.

The position of the maximum of the size distribution $P_R(t, r_p)$ varies with the parameter α . Comparing the definition of $U_{0L,0R}$ in the equation (5) with the potential (1), we see that the field intensity at the membrane is $|E|^2 \sim 1/\alpha^3$. Thus, the powers of the laser beams that excite the left and right membranes are also scaled as $W_L \sim 1/\alpha^3$ and $W_R \sim 1/\alpha^3$. In other words, if the parameter α increases, the maximum of the size distribution function shifts to larger r_p , and the required powers W_L, W_R decrease as $1/\alpha^3$. This obvious scaling law gives us the possibility to tune to any size of the target particles by simply changing the intensities W_L, W_R while keeping their ratio constant. Then, the sorting time increases proportionally to α because of the scaling law of t_0 in Eq. (4).

Figure 8(a) shows the time evolution of the size distribution function $P_R(t, r_p)$ when solving the 3D Fokker-Planck equation (2) for incident wave intensities $W_L = 14 \text{ mW}/\mu\text{m}^2$ and $W_R = 23.3 \text{ mW}/\mu\text{m}^2$, $W_R/W_L = 5/3$. Figure 8(b) is the same Fig. 8(a), but for $W_L = 0.014 \text{ mW}/\mu\text{m}^2$ and $W_R = 0.0233 \text{ mW}/\mu\text{m}^2$. At the same time, as before, $W_R/W_L = 5/3$. Reducing the power by a factor of 1000 led to a shift of the distribution function towards larger sizes. Meanwhile, in the

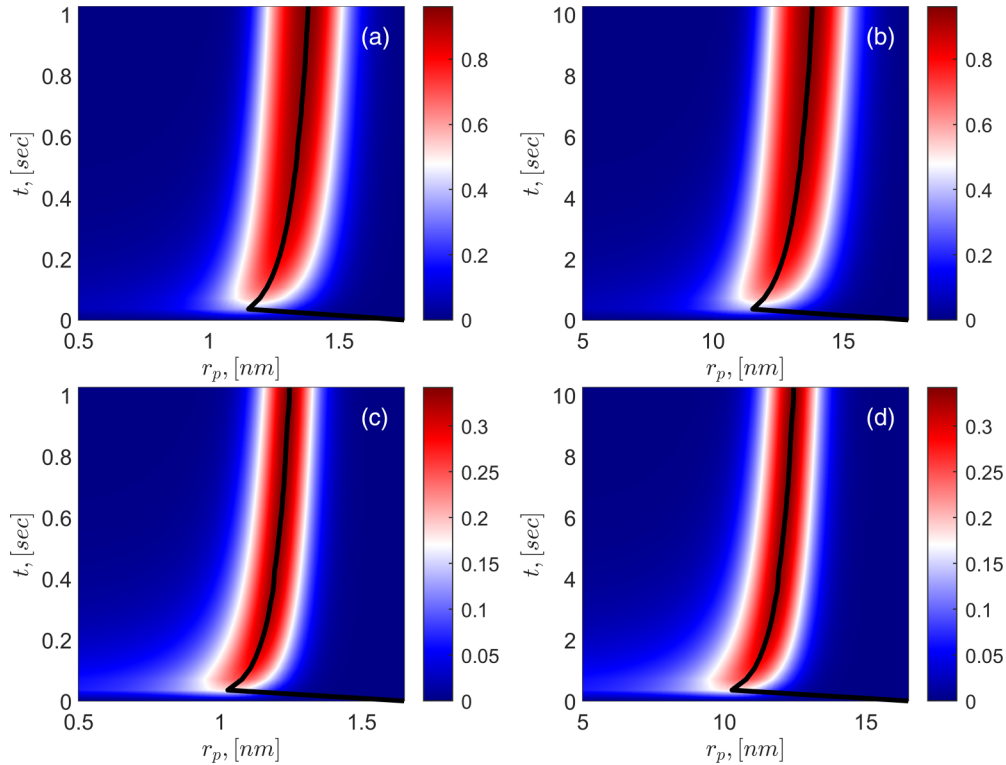


FIG. 8. Solutions of the 3D Fokker-Planck equation (2) $P_R(t, r_p)$ (3) at different laser powers W_L, W_R , corresponding to potential depths $U_{0L} = 3k_B T, U_{0R} = 5k_B T$: $W_L = 14 \text{ mW}/\mu\text{m}^2$ and $W_R = 23.3 \text{ mW}/\mu\text{m}^2$ for $r_p = 1 \text{ nm}$ (a), $W_L = 0.014 \text{ mW}/\mu\text{m}^2$ and $W_R = 0.0233 \text{ mW}/\mu\text{m}^2$ for $r_p = 10 \text{ nm}$ (b). Solutions, corresponding to potential depths $U_{0L} = 5k_B T, U_{0R} = 5k_B T$: $W_L = 23.3 \text{ mW}/\mu\text{m}^2$ and $W_R = 23.3 \text{ mW}/\mu\text{m}^2$ for $r_p = 1 \text{ nm}$ (c), $W_L = 0.0233 \text{ mW}/\mu\text{m}^2$ and $W_R = 0.0233 \text{ mW}/\mu\text{m}^2$ for $r_p = 10 \text{ nm}$ (d). The black line shows the dependence of the maximum of the distribution P_R on time.

first case of higher intensities the maximum of the distribution function at the final time point was tuned to 1.4 nm, in the second case of lower intensities it was tuned to 14 nm, and the sorting time also increased by a factor of 10. Figures 8(c) and 8(d) show the distributions of $P_R(t, r_p)$ at $W_R/W_L = 1$. These figures confirm the conclusion from the 1D calculations shown in Fig. 7 that the ratio W_R/W_L needs to be optimized for efficient sorting.

Our investigations show that the sorting process is robust to changes in the system dimensions, i.e., the distance between the membranes and the length of regions I, III, and V, with only the sorting time changing. An important practical point is that the distribution function reaches quasi-stationary state very quickly, and then changes slowly with time. This means that it is not necessary to strictly fix the sorting completion time.

IV. CONCLUSIONS AND DISCUSSIONS

We propose a sorting mechanism based on the Brownian motion under the influence of optical forces. The Ashkin force corresponds to a potential well with depth of several $k_B T$ for the target particle size. The sorting system shown in Fig. 1 consists of two parallel membranes engineered to support a special type of symmetry-protected bound state in the continuum (SP BIC). One special feature of the SP BIC is that the EM field is concentrated in the membrane holes. By exciting the SP BIC in the left and right membranes with laser beams of different powers W_L and W_R , we set up a device capable of accumulating particles of certain sizes in the holes of the right membrane. The size distribution of the captured particles depends on the ratio of applied powers W_R/W_L . As seen in Fig. 7, the ratio $W_R/W_L = 5/3$ can be considered optimal from the point of view of narrow distribution width and sorting efficiency.

It should be noted that the proposed mechanism for separating the particle fractions is based on a significantly nonequilibrium process. Indeed, without an initial concentration gradient, Brownian motion would not result in the transfer of particles from left to right. In addition, the sorting time is limited because at equilibrium the nanoparticles are distributed according to Boltzmann's law $P \sim \exp(-U(\mathbf{r})/k_B T)$. Therefore, the process of sorting and unloading the sorted nanoparticles should be performed rather quickly.

Figure 7 illustrate the resulting distribution over the radii of spherical nanoparticles in the right membrane. This distribution have a width ($\pm 30\%$). Therefore, the proposed method is more suitable for a mixture of only a few types of nanoparticles whose radii are well separated by values exceeding at least the width of the probability distribution. In particular, a mixture of nanoparticles with sizes of 0.5, 1.5, and 2.5 nanometers could be well separated by the presented method.

The proposed mechanism allows to capture particles whose sizes are distributed in some narrow but finite range, as shown in Fig. 7. To narrow down the probability distribution of this fraction, the particles collected by the right membrane can be used as a starting mixture for the next step of the sorting process. Using refining procedures in sequence can help making the probability distribution very sharp.

We assumed the room temperature of $T = 300$ K for the sorting process. A simple energy balance between the input power of the laser beams and the power dissipated by thermal conduction gives a heating estimate of $\Delta T \approx 5$ K, primarily because of the low absorption of water and silicon at the wavelength $\lambda = 1.55 \mu\text{m}$. Our calculations show a nice stability of the sorting process in relation to increase of temperature, because the important quotient $U_0/k_B T$ changes slightly. This means that we can neglect the temperature degradation during the sorting.

For simplicity, we have represented particles as spherical isotropic dielectrics defined only by radius and permittivity, see Eq. (1). Nevertheless, there is no limitation for sorting nanoparticles of arbitrary shape by their individual polarizability, which can be calculated in the dipole approximation.

The hole in the membranes were designed to be square, although other shapes, such as circles, could be used. From a practical standpoint, round holes are easier to manufacture and can provide structural integrity to the system. The basic requirements for the membrane remain the same, i.e., it must support a SP BIC with maximum field intensity inside the holes and allow for free passage of particles.

There are some difficulties, which are worth to be discussed briefly. First, the accumulation of nanoparticles in holes of membranes distorts the BIC field [30,35] and shift the BIC frequency. After trapping of a large number of nanoparticles the resonant condition may be violated. To estimate this effect qualitatively, we use the perturbation theory [57]

$$\Delta\omega_c = -\omega\overline{\Delta\varepsilon}, \quad (6)$$

where $\overline{\Delta\varepsilon}$ is the change in permittivity because of N nanoparticles with a volume $V_p = 4N\pi r_p^3/3$ averaged over the volume of the hole $V_h = a^2H$,

$$\Delta\varepsilon = (V_p\varepsilon_p + (V_h - V_p)\varepsilon_l)/V_h - \varepsilon_l = (\varepsilon_p - \varepsilon_l)V_p/V_h.$$

The resonant condition is broken if $\Delta\omega_c > \omega_c/Q$. For the sizes of holes applied in the paper, the number of 1 nm nanoparticles in each hole should not exceed one thousand.

Second, each membrane has finite dimensions along the x and y directions, which leads to formation of a standing wave in the EM field envelope function [58]. This, in turn, means that the depth of the potential wells will be different in each cell. As a result, particles of different sizes will accumulate in the right membrane. To reduce the inhomogeneity of the potential, only the central part of the extended membrane can be used, where the depth of the potential wells varies slightly.

One of the challenges in the proposed scheme is that the sorting process is not continuous. The sorting process can be made continuous by replacing each membrane with a complex of two parallel membranes. This complex must support a high-Q state whose EM field is concentrated between the membranes, where particles will accumulate. By using a continuous flow of liquid between the membranes to carry away these particles, we will create a device that does not require to stop the sorting to unload the sorted particles.

Our investigation is purely theoretical, and many other challenging factors that may arise during experimental implementation have not been considered. The main idea of the

study is that it is possible to employ Brownian motion for sorting ultrasmall particles when the particles are subjected to a strong optical potential, thanks to the nearfield resonant mode with a high Q factor. The competition between the optical and stochastic forces, one of which tending to localize the particle and the other to delocalize it, produces the sorting effect. Despite possible limitations imposed by the

experimental implementation, we are convinced that the proposed sorting mechanism can be used in practice.

ACKNOWLEDGMENTS

The work was supported by Russian Science Foundation Grant No. 22-12-00070.

- [1] W. Cai, E. Wang, P.-W. Chen, Y.-H. Tsai, L. Langouche, and Y.-H. Lo, A microfluidic design for desalination and selective removal and addition of components in biosamples, *Biomicrofluidics* **13**, 024109 (2019).
- [2] H. Xin, Y. Li, Y. Liu, Y. Zhang, Y. Xiao, and B. Li, Optical forces: From fundamental to biological applications, *Adv. Mater.* **32**, 2001994 (2020).
- [3] R. P. Badman, F. Ye, and M. D. Wang, Towards biological applications of nanophotonic tweezers, *Curr. Opin. Chem. Biol.* **53**, 158 (2019).
- [4] S. A. Meek, H. Conrad, and G. Meijer, Trapping molecules on a chip, *Science* **324**, 1699 (2009).
- [5] S. Lin, J. Hu, L. Kimerling, and K. Crozier, Design of nanoslot-photonic crystal waveguide cavities for single nanoparticle trapping and detection, *Opt. Lett.* **34**, 3451 (2009).
- [6] Y.-F. Chen, X. Serey, R. Sarkar, P. Chen, and D. Erickson, Controlled photonic manipulation of proteins and other nanomaterials, *Nano Lett.* **12**, 1633 (2012).
- [7] J. Ma, L. J. Martinez, and M. L. Povinelli, Optical trapping via guided resonance modes in a Slot-Suzuki-phase photonic crystal lattice, *Opt. Express* **20**, 6816 (2012).
- [8] C. Ciminelli, D. Conteduca, F. Dell’Olio, and M. N. Armenise, Design of an optical trapping device based on an ultra-high Q/V resonant structure, *IEEE Photon. J.* **6**, 0600916 (2014).
- [9] S. Hu, M. Khater, R. Salas-Montiel, E. Kratschmer, S. Engelmann, W. Green, and S. Weiss, Experimental realization of deep-subwavelength confinement in dielectric optical resonators, *Sci. Adv.* **4**, aat2355 (2018).
- [10] H. Zhao, L. K. Chin, Y. Shi, K. T. Nguyen, P. Y. Liu, Y. Zhang, M. Zhang, J. Zhang, H. Cai, E. P. H. Yap, W. Ser, and A.-Q. Liu, Massive nanophotonic trapping and alignment of rod-shaped bacteria for parallel single-cell studies, *Sens. Actuators B: Chemical* **306**, 127562 (2020).
- [11] Y. Shi, H. Zhao, L. K. Chin, Y. Zhang, P. H. Yap, W. Ser, C.-W. Qiu, and A. Q. Liu, Optical potential-well array for high-selectivity, massive trapping and sorting at nanoscale, *Nano Lett.* **20**, 5193 (2020).
- [12] S. S. Hou, Y. Liu, W. X. Zhang, and X. D. Zhang, Separating and trapping of chiral nanoparticles with dielectric photonic crystal slabs, *Opt. Express* **29**, 15177 (2021).
- [13] H. Ren, H. Luo, M. A. Selim, G. G. Pyrialakos, F. O. Wu, M. Khajavikhan, and D. Christodoulides, Rigorous analysis of optical forces in dielectric structures based on the Minkowski-Helmholtz formula, *Phys. Rev. A* **106**, 033517 (2022).
- [14] B. Shi, Y. Cao, T. Zhu, H. Li, Y. Zhang, R. Feng, F. Sun, and W. Ding, Multiparticle resonant optical sorting using a topological photonic structure, *Photonics Res.* **10**, 297 (2022).
- [15] W. Kim, Ş. K. Özdemir, J. Zhu, L. He, and L. Yang, Demonstration of mode splitting in an optical microcavity in aqueous environment, *Appl. Phys. Lett.* **97**, 071111 (2010).
- [16] Y. Li, O. Svitelskiy, A. Maslov, D. Carnegie, E. Rafailov, and V. Astratov, Giant resonant light forces in microspherical photonics, *Light: Sci. Appl.* **2**, e64 (2013).
- [17] S. Yang and J. C. Ndukaife, Optofluidic transport and assembly of nanoparticles using an all-dielectric quasi-BIC metasurface, *Light Sci. Appl.* **12**, 188 (2023).
- [18] H. Wang, Z. Han, L. Zhang, and J. Chen, Morphology-dependent resonance induced optical forces in a multiple-sphere system, *Opt. Express* **31**, 9996 (2023).
- [19] B. S. Schmidt, A. H. J. Yang, D. Erickson, and M. Lipson, Optofluidic trapping and transport on solid core waveguides within a microfluidic device, *Opt. Express* **15**, 14322 (2007).
- [20] D. Erickson, X. Serey, Y.-F. Chen, and S. Mandal, Nanomanipulation using near field photonics, *Lab Chip* **11**, 995 (2011).
- [21] A. V. Maslov, Resonant optical propulsion of a particle inside a hollow-core photonic crystal fiber, *Opt. Lett.* **41**, 3062 (2016).
- [22] M. I. Antonoyiannakis and J. B. Pendry, Mie resonances and bonding in photonic crystals, *Europhys. Lett.* **40**, 613 (1997).
- [23] V. Liu, M. Povinelli, and S. Fan, Resonance-enhanced optical forces between coupled photonic crystal slabs, *Opt. Express* **17**, 21897 (2009).
- [24] J. Zhang, K. F. MacDonald, and N. I. Zheludev, Giant optical forces in planar dielectric photonic metamaterials, *Opt. Lett.* **39**, 4883 (2014).
- [25] C. B. R. Hurtado, J. Dickmann, F. F. Bruns, T. Siefke, and S. Kroker, Bound states in the continuum for optomechanical light control with dielectric metasurfaces, *Opt. Express* **28**, 20106 (2020).
- [26] E. N. Bulgakov and A. F. Sadreev, Resonant bending of silicon nanowires by incident light, *Opt. Lett.* **45**, 5315 (2020).
- [27] S. Yang, C. Hong, Y. Jiang, and J. Ndukaife, Nanoparticle trapping in a quasi-BIC system, *ACS Photonics* **8**, 1961 (2021).
- [28] J. Wang, Z. Han, C. Wang, and H. Tian, Parallel trapping of multiple nanoparticles using a quasi-bound state in the continuum mode, *J. Opt. Soc. Am. B* **39**, 2356 (2022).
- [29] L. Mao, P. Cheng, K. Liu, M. Lian, and T. Cao, Sieving nanometer enantiomers using bound states in the continuum from the metasurface, *Nanoscale Adv.* **4**, 1617 (2022).
- [30] E. N. Bulgakov and A. F. Sadreev, Self-trapping of nanoparticles by bound states in the continuum, *Phys. Rev. B* **106**, 165430 (2022).
- [31] H. Qin, Y. Shi, Z. Su, G. Wei, Z. Wang, X. Cheng, A. Q. Liu, P. Genevet, and Q. Song, Exploiting extraordinary topological optical forces at bound states in the continuum, *Sci. Adv.* **8**, ade7556 (2022).

- [32] H. Qin, W. Redjem, and B. Kante, Tunable and enhanced optical force with bound state in the continuum, *Opt. Lett.* **47**, 1774 (2022).
- [33] E. Bulgakov and A. Sadreev, Precise size sorting of nanoparticles by bound states in the continuum in a dual finite grating, *Opt. Lett.* **48**, 4705 (2023).
- [34] L. Huaiqing, C. Feng, J. Youchao, F. Maosheng, N. Yao, F. Yijiao, and Z. Xiancun, Giant enhanced optical force in silicon elliptical nanopillars assisted by quasi-BIC, *IEEE Photonics Technol. Lett.* **35**, 485 (2023).
- [35] A. Kostyukov, V. Gerasimov, A. Ershov, E. Bulgakov, and A. Sadreev, Size-selective optical trapping of nanoparticles with bound states in the continuum, *Opt. Lasers Eng.* **171**, 107797 (2023).
- [36] P. Paddon and J. F. Young, Two-dimensional vector-coupled-mode theory for textured planar waveguides, *Phys. Rev. B* **61**, 2090 (2000).
- [37] T. Ochiai and K. Sakoda, Dispersion relation and optical transmittance of a hexagonal photonic crystal slab, *Phys. Rev. B* **63**, 125107 (2001).
- [38] W. Suh, M. F. Yanik, O. Solgaard, and S. Fan, Displacement-sensitive photonic crystal structures based on guided resonance in photonic crystal slabs, *Appl. Phys. Lett.* **82**, 1999 (2003).
- [39] C. P. Ho, P. Pitchappa, P. Kropelnicki, J. Wang, H. Cai, Y. Gu, and C. Lee, Two-dimensional photonic-crystal-based Fabry-Perot etalon, *Opt. Lett.* **40**, 2743 (2015).
- [40] L. Li and H. Yin, Bound states in the continuum in double layer structures, *Sci. Rep.* **6**, 26988 (2016).
- [41] J. M. Fitzgerald, S. K. Manjeshwar, W. Wiczorek, and P. Tassin, Cavity optomechanics with photonic bound states in the continuum, *Phys. Rev. Res.* **3**, 013131 (2021).
- [42] S. Xie, S. Xie, Z. Li, Z. Li, G. Tian, J. Zhan, and Q. Liu, High-Q resonances governed by bound states in the continuum of a cross-shape nanohole array perforated on a photonic crystal slab, *Optik* **243**, 167449 (2021).
- [43] D. Liu, X. Yu, F. Wu, W. Du, L. Chen, F. Liu, M. Kuwahara, and S. Ono, Terahertz asymmetric metallic hole arrays with polarization-independent quasi-bound states in the continuum for membrane sensing, *Opt. Express* **31**, 23608 (2023).
- [44] L. Huang, S. Li, C. Zhou, H. Zhong, S. You, L. Li, Y. Cheng, and A. E. Miroshnichenko, Realizing ultrahigh-Q resonances through harnessing symmetry protected bound states in the continuum, *Adv. Funct. Mater.* **34**, 2309982 (2023).
- [45] T. A. J. Duke and R. H. Austin, Microfabricated sieve for the continuous sorting of macromolecules, *Phys. Rev. Lett.* **80**, 1552 (1998).
- [46] I. Ricárdez-Vargas, P. Rodríguez-Montero, R. Ramos-García, and K. Volke-Sepúlveda, Modulated optical sieve for sorting of polydisperse microparticles, *Appl. Phys. Lett.* **88**, 121116 (2006).
- [47] F. Nan and Z. Yan, Optical sorting at the single-particle level with single-nanometer precision using coordinated intensity and phase gradient forces, *ACS Nano* **14**, 7602 (2020).
- [48] H. Zhao, L. K. Chin, Y. Shi, P. Y. Liu, Y. Zhang, H. Cai, E. P. H. Yap, W. Ser, and A.-Q. Liu, Continuous optical sorting of nanoscale biomolecules in integrated microfluidic-nanophotonic chips, *Sens. Actuators B: Chem.* **331**, 129428 (2021).
- [49] L. Novotny and B. Hecht, *Principles of Nano-Optics* (Cambridge University Press, Cambridge, 2012).
- [50] Y. Harada and T. Asakura, Dynamics and dynamic light-scattering properties of Brownian particles under laser radiation pressure, *Pure and Appl. Optics: J. European Opt. Soc. A* **7**, 1001 (1998).
- [51] T. Davis, Brownian diffusion of nano-particles in optical traps, *Opt. Express* **15**, 2702 (2007).
- [52] M. Zaman, P. Padhy, and L. Hesselink, Fokker-Planck analysis of optical near-field traps, *Sci. Rep.* **9**, 9957 (2019).
- [53] C. Zhou, S. Li, Y. Wang, and M. Zhan, Multiple toroidal dipole Fano resonances of asymmetric dielectric nanohole arrays, *Phys. Rev. B* **100**, 195306 (2019).
- [54] U. Fano, Effects of configuration interaction on intensities and phase shifts, *Phys. Rev.* **124**, 1866 (1961).
- [55] A. E. Miroshnichenko, S. Flach, and Y. S. Kivshar, Fano resonances in nanoscale structures, *Rev. Mod. Phys.* **82**, 2257 (2010).
- [56] E. Kamenetskii, A. Sadreev, and A. Miroshnichenko, *Fano Resonances in Optics and Microwaves: Physics and Applications* (Springer International Publishing, Princeton, NJ, 2018).
- [57] P. Lalanne, W. Yan, K. Vynck, C. Sauvan, and J.-P. Hugonin, Light interaction with photonic and plasmonic resonances, *Laser Photonics Rev.* **12**, 1700113 (2018).
- [58] M.-S. Hwang, H.-C. Lee, K.-H. Kim, K.-Y. Jeong, S.-H. Kwon, K. Koshelev, Y. Kivshar, and H.-G. Park, Ultralow-threshold laser using super-bound states in the continuum, *Nat. Commun.* **12**, 4135 (2021).